The role of local buckling in the determination of H.S.S. rotational capacity

Elsy Saloumi[1], Marielle Hayeck[2], Joanna Nseir[3], Nicolas Boissonnade[4]

Abstract

The present paper focuses on the rotational capacity of H.S.S. steel sections; in particular, the influence of local buckling is accounted for by means of a new generalized cross-sectional slenderness parameter, which is used to characterize the cross-sectional rotational capacity, and, by extension, the available deformation capacity.

Careful shell modelling of hollow section beams in bending was used, the numerical models being previously carefully validated against more than 50 bending tests. Extensive F.E. studies were consecutively performed, including many parameters such as various material grades, load and support arrangements, length-to-height ratios, etc. Specific attention was paid to the introduction of initial geometrical (local) imperfections, as they were shown quite influential on the rotation capacity.

The paper then analyses the numerical results and points out the various influences of height-to-width ratio, shear, moment gradient, yield stress and length-to-height ratio on the available rotational capacity. In a second step, the rotational capacity demand vs. stability criterion is detailed, and related to the proposed generalized cross-sectional slenderness, which is shown to be more appropriate than the b / t ratios usually proposed in design codes. Finally, code-ready recommendations for new ways of allowing for plastic analysis in practical design following the proposed approach are given.

1 Introduction

This paper examines the relationships between local buckling and rotational capacity, in the particular case of H.S.S. profiles. For sections under bending moment actions, rotational capacity can be seen as a measure of ductility, since both can be defined as the ability for a section to undergo large deformations beyond the elastic range while maintaining their – plastic – resistance (see definitions of the rotational capacity R_{cap} in Eq. (1) and Fig. 1). Classically characterized though an infinite horizontal plateau on the σ-ε diagram of carbon steel, both shall be associated to *resistance* (reaching a limited, definite F_y) without stiffness (tangent modulus $E_t = 0$).

---

[1] PhD, <elsysaloumi@gmail.com>
[2] PhD, <marielle_hayeck@hotmail.com>
[3] Professor, Saint-Joseph University, E.S.I.B., <joanna.nseir@usj.edu.lb>
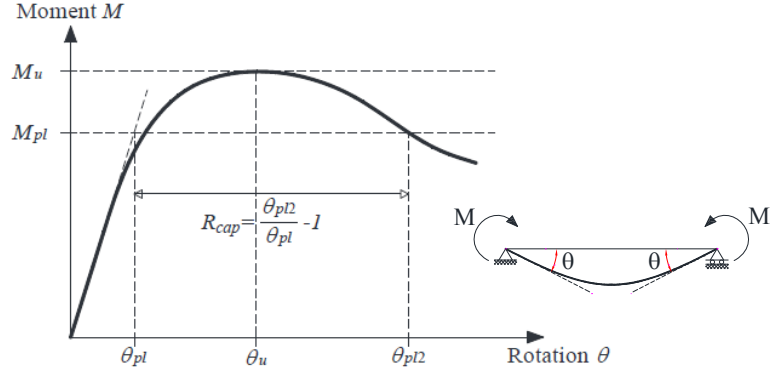[4] Professor, Laval University, <nicolas.boissonnade@gci.ulaval.ca>

Figure 1: Definition of the rotational capacity of a section

$$R_{cap} = \frac{\theta_{pl2} - \theta_{pl}}{\theta_{pl}} = \frac{\theta_{pl2}}{\theta_{pl}} - 1 \qquad (1)$$

In contrast, *elastic buckling – local buckling* in the present context –, can be described as the moment where the section, possessing a certain stiffness associated to the Young's modulus E, suddenly loses rigidity and undergoes an infinite number of possible equilibrium states. All along this way, stresses are not limited in magnitude and can in particular reach levels way beyond the material's yield stress, as elastic stability theory assumes a perfect material, i.e. the stress-strain relationship is elastic linear and stresses can even reach infinity.

Albeit seemingly disconnected, these two concepts are both influencing the behaviour and response of practical steel sections and members, which makes them crucial to understand and master for a sound design. Usually, they are associated in the definition of a so-called relative slenderness λ_{rel} (cf. Eq. (2)) that aims at taking the balance between the influence of ductility/resistance on one side, and the effects of buckling on the other side.

$$\lambda_{rel} = \sqrt{\frac{F_y}{\sigma_{cr}}} \qquad (2)$$

Accordingly, small values of λ_{rel} can be associated to ductile behaviour (compact sections), while large values of λ_{rel} characterize a predominant buckling response, i.e. the occurrence of premature local buckling.

This resistance-stability relationship has been used for decades (Merchant, 1954), and stands as the corner stone of the recently-developed Overall Interaction Concept (O.I.C., see Boissonnade 2017, Hayeck 2018, Boissonnade 2014), as Fig. 2 illustrates.

Step 1: R_{pl} *Load ratio to reach the plastic 'resistance' limit*

Step 2: R_{cr} *Load ratio to reach the critical 'instability' limit*

Step 3: $\lambda_{rel} = \sqrt{\dfrac{R_{pl}}{R_{cr}}}$

Step 4: $\chi = f°(\lambda_{rel})$

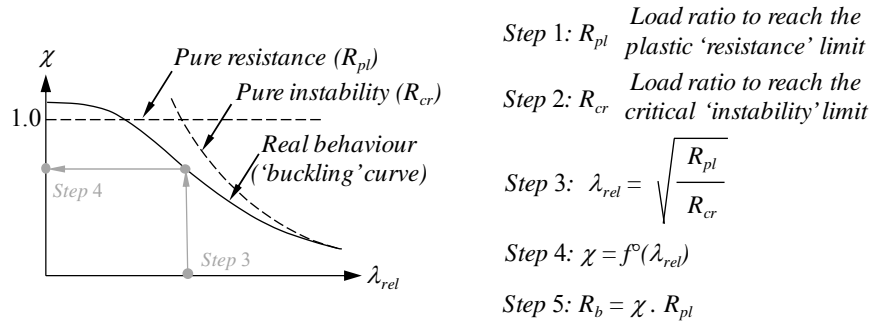Step 5: $R_b = \chi \cdot R_{pl}$

Figure 2: Basic principles and application steps of the O.I.C.

The O.I.C. further extends the concept of relative slenderness to combined loading situations through the use of so-called load ratios, and makes use of buckling curves to provide a direct resistance prediction – steps 4 and 5. Note that in the particular case of section resistance, reference shall be made to *local* buckling, i.e. $\lambda_{rel} \equiv \lambda_L$ where λ_L is the local cross-section relative slenderness as defined in Fig. 2. As λ_L characterizes section sensitivity to local buckling, the usual preliminary classification step is no more necessary; in addition, relying on continuous buckling curves allows for smooth resistance transitions from plastic to slender capacities. These two features allow to fix a series of issues associated to the concept of discrete behavioural classes (Boissonnade 2017, Hayeck 2018, Boissonnade 2014, Chen 2013) that is still of application in major design standards (Eurocode 3 2005, AISC 2010, AS 4100 1998).

Disregarding the classification concept and its b / t limit ratios consequently also removes the criterion that allows – or not – designers to resort to a plastic analysis of their structure. The key point being to assert that a sufficient level of ductility is met to allow for the development of a plastic collapse mechanism, suggestion is made here to rely on λ_L values to characterize the ductility reserves in H.S.S. sections: as recalled previously, although λ_L is often used solely to provide information relative to buckling, it may also effectively be used as a measure of ductility, and, by association, of the rotational capacity. Accordingly, the present paper establishes how λ_L can be related to the rotational capacity R_{cap} of H.S.S. sections, and eventually uses these relationships to provide code-ready recommendations allowing for plastic analysis.

This approach however cannot fully replace the real, natural criterion that should prevail when the question comes to whether or not a plastic mechanism may develop. This criterion is recalled in Fig. 3, and clearly shows that identifying the demand in rotation capacity R_{dem} is as important as evaluating R_{cap}, i.e. that relying solely on R_{cap} is insufficient.
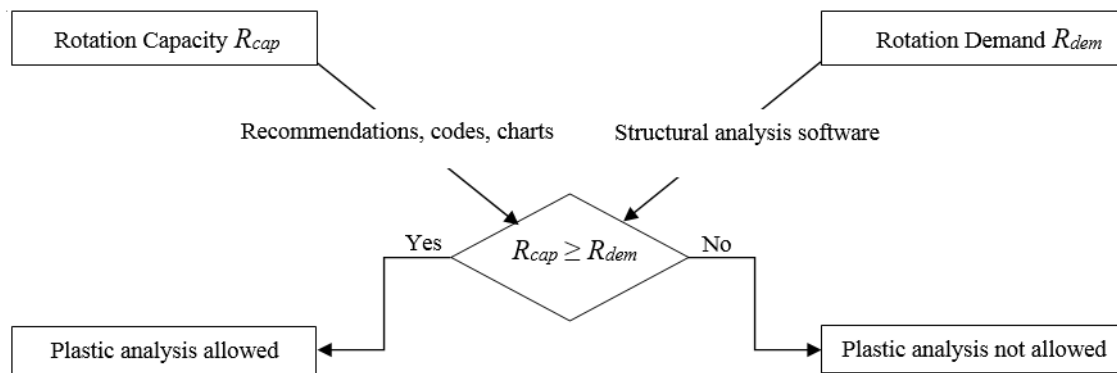

Figure 3: Criterion to allow for plastic analysis

The need to characterize R_{dem} as well was evidenced by many papers and reports (see for example Kuhlmann 1989, Stranghoner 1004, Lay 1967, Kemp 1984, Kato 1989, Ziemian 1992, Ricles 1998, Wilkinson 1999). However, since the required rotation – or rotation demand R_{dem} – differs with the loading and geometry of the considered structure and because the calculation of R_{dem} for complex structures can sometimes be complicated, time consuming and unreliable (Galambos 1968, Yura 1978), a fixed value of R_{dem} is usually prescribed as a minimum plastic rotation requirement in practical design.

Several such R_{dem} values can be traced back in the relevant literature. In a non-exhaustive manner, one can refer to the Eurocode 3 Editorial Group (1989) who suggested that a value $R_{dem} = 3$ was suitable for plastic design, while Korol and Hudoba (1972) recommended a value of $R_{dem} = 4$. Hasan and Hancock (1989) and Zhao and Hancock (1991) used a limitation of

R_{dem} = 4 to determine suitable plastic slenderness for the Australian Standard AS 4100 (1998). Kuhlmann (1989) and Neal (1977) suggested that a value of R_{dem} = 2 was sufficient for continuous beams. Stranghöner, Sedlacek and Boeraeve (1994) investigated the behavior of hollow sections and outlined that different rotation requirements are necessary than for I-sections, and they found that R_{dem} = 3 was adequate for continuous beams.

In accordance with the underlying concepts of current Eurocode 3 (1989), a value R_{dem} = 3 was kept as a reference in the following – this value can indeed be shown to be usually conservative. Emphasis shall therefore be kept on R_{cap} only to provide an alternative criterion for plastic analysis that consists in ensuring that R_{cap} > 3.

Typical $R_{cap} = f°(\lambda_L)$ relationships are then finally needed, and this shall consist in a rather complex task, as Fig. 4 shows: the latter summarizes a large number of experimental bending tests and plots the recorded R_{cap} values as a function of the dominant plate slenderness in the section λ_p – these data have served as the background to current b / t limits ratios in Eurocode 3. As can be seen, a very large scatter is reported, pointing out various parameters to be of significant influence, such as the fabrication process (hot-rolled HR vs. cold-formed CF) or the test configuration (3-point bending 3pt vs. 4-point 4-pt arrangements). Also, the dispersion of the results also questions the need to identify additional parameters, since, for a given λ_p, R_{cap} may take extremely different values, sometimes varying more than in a factor 10.
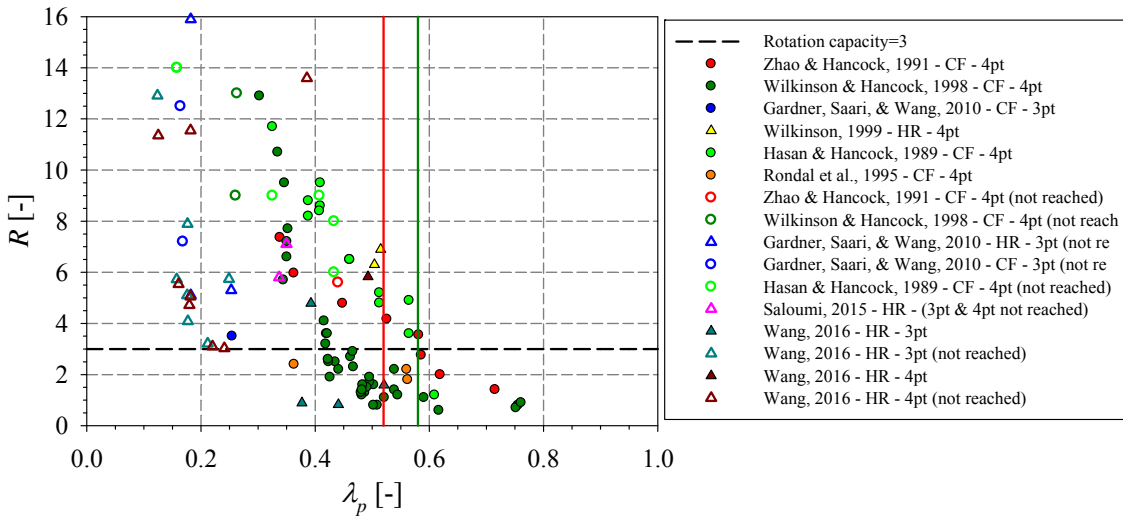

Figure 4: R_{cap} as a function of plate slenderness λ_p, experimental data

This further emphasizes the need for large databases, covering a wide range of key parameters. This nowadays is usually achieved through extensive F.E. simulations that are capable of providing large databases of reliable results, while also allowing isolating the single influence of a given parameter. Accordingly, the following typical methodology was followed through the present research:

- Performance and collection of well-documented test data;
- Development and validation of shell F.E. models against experimental results;
- Extensive numerical parametric studies;
- Development and assessment of new design criteria in the form $R_{cap} = f°(\lambda_L) > 3.0$.

In this respect, a series of 23 bending tests on hot-formed and cold-formed H.S.S. was performed; detailed results and analysis can be found in Saloumi (2016) and Saloumi (2017). Also, a series of 32 tests performed in Sydney by Wilkinson (1999) with all the necessary

detailed data could be made available, and both have served in the validation of dedicated shell F.E. models that are described in Section 2. In particular, specific investigations related to the sensitivity of R_{cap} to geometrical imperfections are reported in § 2.2. Section 3 presents the results of extensive numerical parametric studies, where the various influences of height-to-width h / b aspect ratio, load application and moment gradient, length-to-height L / h ratio, steel grade and fabrication process are analysed. Eventually, paragraph 4 summarizes the various observations into code-ready $R_{cap} = f°(\lambda_L)$ relationships that shall be used to allow – or not – resorting to a plastic analysis.

2 Shell F.E. models

2.1 Basic modelling considerations, material, loading and support conditions

All numerical simulations relied on software FINELg (1999), continuously developed at the University of Liège and Greisch Design Office since 1970. Use of quadrangular 4-nodes plate-shell finite elements with typical features (Corotational Total Lagrangian formulation, Kirchhoff's theory for bending) has been made; mesh sensitivity analyses have been performed and adequate numbers of integration points in-plane and across the thickness have also been adopted (Saloumi 2016).

Material response of carbon steel was modelled through various σ-ε relationships, depending on the fabrication process and on the location of the considered fibre in the section. Hot-rolled sections typically accounted for steel behaviour through 4-segments approximations (Fig. 5), as recommended by Yun et al. (2017), who relied on thousands of tensile test results to provide best-fitted positions and slopes of the various segments, as a function of the steel grade.

This allowed to account for strain hardening reserves and large strains, which are crucial aspects with respect to the characterisation of the rotational capacity. Fig. 5 plots the typical stress-strain relationships adopted in the numerical studies (cf. § 3) for the steel grades considered herein.
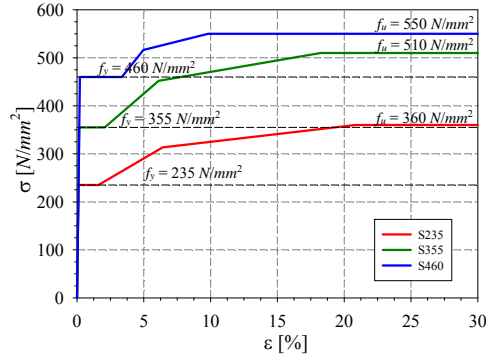

Figure 5: Hot-formed material model considered for different steel grades

Distinctions between flat faces and corner fibres were made in the case of cold-formed H.S.S. Flat faces were characterised by a typical Ramberg-Osgood equation (Hayeck 2015), while the corner areas relied on a different material response that accounted for (i) a higher apparent yield stress and (ii) a reduced ductility reserve – Fig. 6a. In order to avoid numerical issues in the non-linear F.E. analyses, a fictitious softening behaviour was accounted for, so that these fibres could allow for larger strains while carrying virtually no stress. Fig. 6b illustrates the cold-formed material behaviour that was taken into account in the present studies – Note the decrease in fracture strain as the yield stress increases.
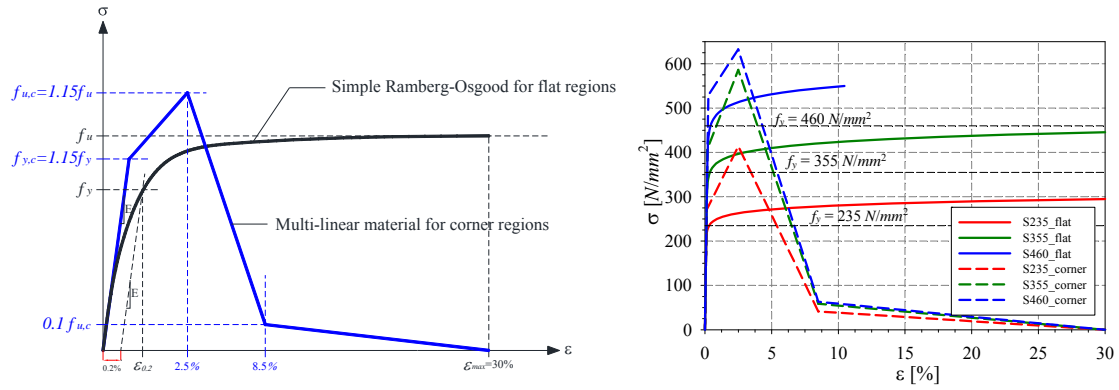
Figure 6: a) Typical stress-strain curves for cold-formed carbon steels; simple Ramberg-Osgood law for flat regions and a multi-linear material model for corner regions – b) Cold-formed material model considered in the flat and corner region for each nominal yield strength

Boundary conditions were modelled so that end sections fulfilled pin-pin assumptions. For hollow sections, this implied the use of a fictitious node at the centre of the end sections (see Fig. 7a), where vertical supports were effectively acting – both in the direction or major and minor axes. This was made possible through the use of kinematic linear constraint conditions that ensured the end sections fulfilled the Bernoulli "plane sections remain plane" assumption and that flexural rotations were effective about the centroid. In addition, torsional twist was prevented, and end section nodes of each plate were transversally fixed in order to avoid any local buckling or bearing potential failure modes at the extremities of the beams (Fig. 7a).
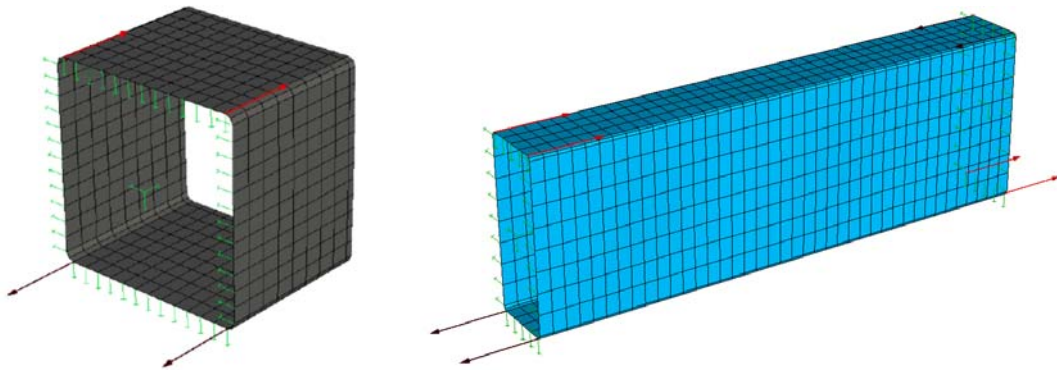

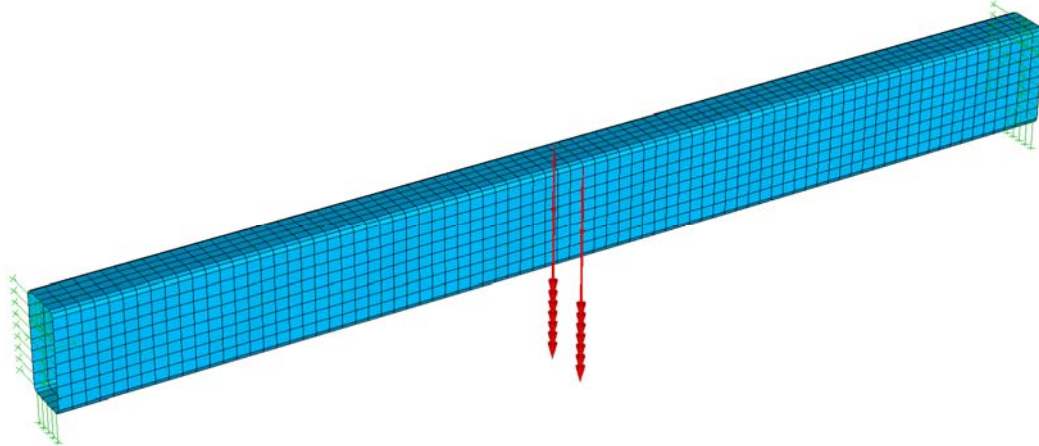Figure 7: a) Boundary conditions at end sections – b) Application of constant bending moment

Figure 8: Modelling of 3-point bending cases

The load cases considered mainly consisted in either constant bending moment, a transverse load at mid-span (3-point bending cases) or in two symmetrically-applied point loads (4-point bending cases). Constant bending moment distributions were made effective through suitable 4 equal point loads at top flange nodes (Fig. 7b), which, thanks to the kinematic linear constraints, were distributed along each end section node so as to meet linear distributions. Point load cases were modelled as Fig. 8 illustrates: in order to avoid any local concentration of stresses in the vicinity of the point load application, the transverse load was evenly distributed along the webs of the section by means of series of nodal forces whose sum equalled the applied point load.

Due residual stresses were also obviously considered. For hot-formed sections, auto-equilibrated *membrane* residual stresses patterns were implemented in the numerical models with a reference yield stress $F_y = 235$ N/mm^2 along with constant residual stresses patterns (Fig. 9). *Flexural* residual stresses were adopted for cold-formed sections with a linear distribution across the thickness. Their magnitude was assumed equal to $1.2 \cdot 235$ N/mm^2 in the flat regions and equal to F_y in the corner regions (see Nseir 2015 and Hayeck 2016 for more details).

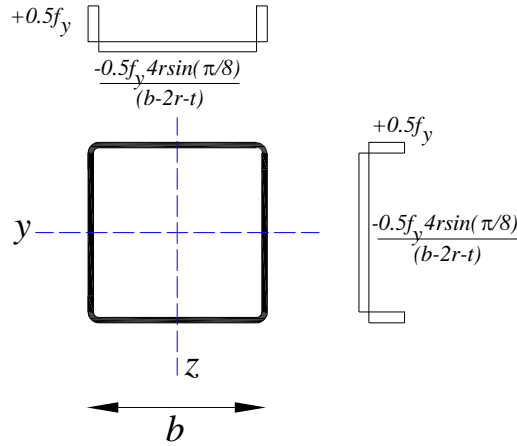

Figure 9: Auto-equilibrated residual stress pattern for hot-formed tubular profiles

2.2 Sensitivity to geometrical imperfections

Geometrical imperfections deserved a particular attention since, as other authors noted (Kuhlmann, 1989), they ought to be associated to the scattering of the results presented in Fig. 4. Accordingly, defining a systematic distribution of geometrical imperfections for parametric studies is a delicate question, as it remains a challenge to define safe yet accurate and realistic patterns when (i) real distributions can be highly variable and potentially any, and (ii) these local defaults are known to cause large changes in R_{cap} (Saloumi 2016, Saloumi 2017).

In this respect, a dedicated small sub-study was undertaken where six different shapes and amplitudes of initial local geometric imperfections were selected (see Fig. 10). Various periods – in green on Fig. 10 – were considered as a function of the sections' dimensions, either through averaged values of flat lengths of webs and flanges (imperfection patterns 1-2-4-5), individual plates (pattern 3) or from the eigenmode (Imp 6). Fig. 11 further illustrates the consequences of such choices on the distribution of imperfections along the member – Note in particular the number of half waves in each plates, sometimes identical (Fig. 11a and 11c), sometimes disconnected (Fig. 11b), i.e. the 90° web-flange angles are lost.
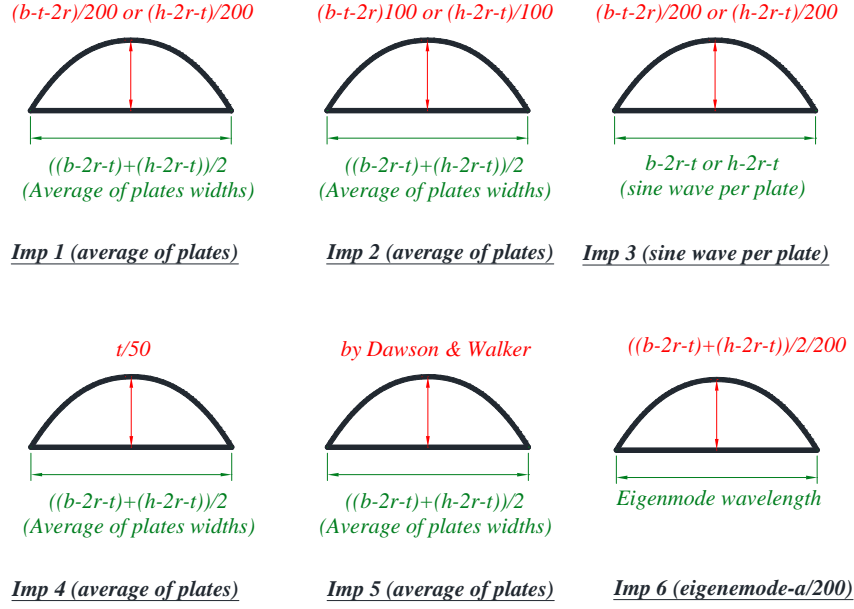
Figure 10: Considered local geometrical imperfections

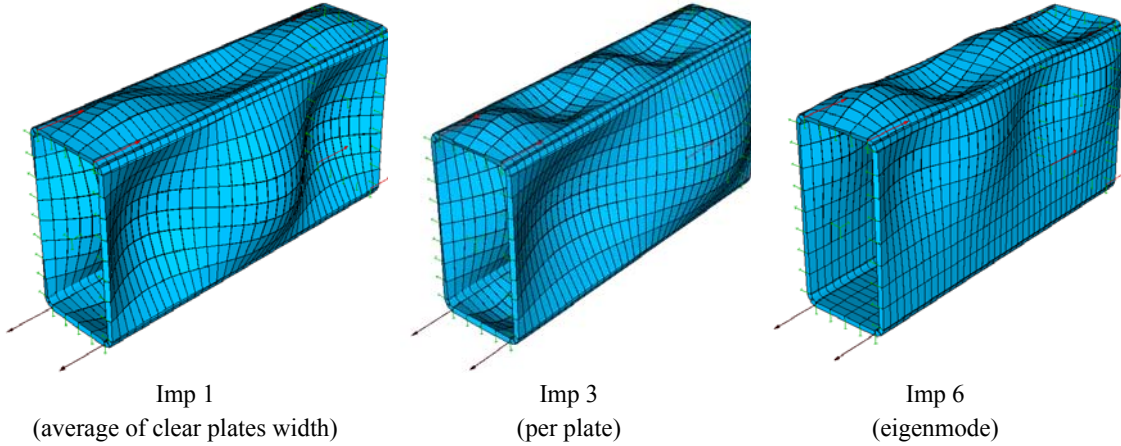| Imp 1	Imp 3	Imp 6
(average of clear plates width)	(per plate)	(eigenmode)

Figure 11: Geometrical imperfections for RHS sections with $h/b = 2$ (magnified)

Amplitudes were varied as well – see indications in red on Fig. 10 –, and were set as functions of the sections' dimensions (imperfection patterns 1-2-3-6), of the thickness (pattern 5) or following the recommendations of Dawson et al. (1972, Imp 5) as amended by Gardner et al. (2010) through the following equations:

$$Amplitude = \beta \cdot \sqrt{\frac{F_y}{\sigma_{cr}}} \cdot t \quad where \; \beta = \begin{cases} 0.028 \; for \; hot\text{-}rolled \; sections \\ 0.034 \; for \; cold\text{-}formed \; sections \end{cases} \quad (3)$$

In Eq. (3), F_y is the yield stress, t the thickness and σ_{cr} the plate critical stress. Accordingly, slightly higher imperfections were assumed for cold-formed sections. No global initial imperfections were introduced as only cross section capacities were examined.

Figs. 12a and 12b provide examples of the obtained results, where the rotational capacity R_{cap} is plotted as a function of the sections' slenderness λ_L, for the 6 various imperfection patterns considered. The figures also report the $R_{cap} = 3$ reference value as well as a $\lambda_L = 0.5$ vertical line which stands the slenderness-based limit underlying the b/t limits ratios in Eurocode 3

8

(1989) to separate class 1 from class 2 sections. Although the figures only show results obtained for hot-rolled tubes, identical conclusions and trends were observed for cold-formed sections, see Saloumi (2016). Figs. 12a and 12b provide the following information:

- Quite large difference in rotational capacities are reported, owing to pronounced steepness of the various curves. These high slopes can be shown to be associated with the plastic plateau in the material curves (Saloumi 2016): yield extend in these fibres is indeed such that strains spread very quickly, and so does R_{cap}, thus the large differences. Lesser steepness was observed for cold-formed H.S.S., albeit still important. This further emphasizes the need for a unique imperfection pattern, for sake of consistency; this also partly explains the large scatters observed in experimental results – see for example Fig. 4;
- Generally, the sensitivity of R_{cap} to imperfections increased as the section slenderness decreased, no matter the section's aspect ratio;
- Both shapes and amplitudes of geometrical imperfections are seen to have a substantial effect on the rotational capacity. As an example, Fig. 12a abrupt curves when $\lambda_L < 0.4$ lead to, at $\lambda_L = 0.4$, rotational capacities varying from 2 to 13;
- Imperfection patterns 4 and 5 lead to noticeably higher rotational capacities, owing to quite small amplitudes. The latter have been calibrated from test data but may not be suitable for systematic patterns used in parametric studies;
- Imp 2 pattern amplitude of $a / 100$ where a is the plate's leading dimensions leads to the lowest R_{cap} values. Although motivation for this study is to choose a safe-sided distribution, an amplitude of $a / 100$ leads to quite severe results and was deemed unreasonable, in addition to lie too far from imperfections' measurements (Nseir 2015). Consequently, this pattern was disregarded;
- Albeit the eigenmode-conform Imp 6 pattern remains widely used, it was not kept any further, since it was considered less appropriate and possibly not guaranteeing safer, conservative results (Nseir 2015).

Accordingly, Imp 1 imperfection pattern was finally chosen: the $a / 200$ amplitude seemed reasonable and an average period between flange and web with an identical number of half-waves in flanges and webs adequate.
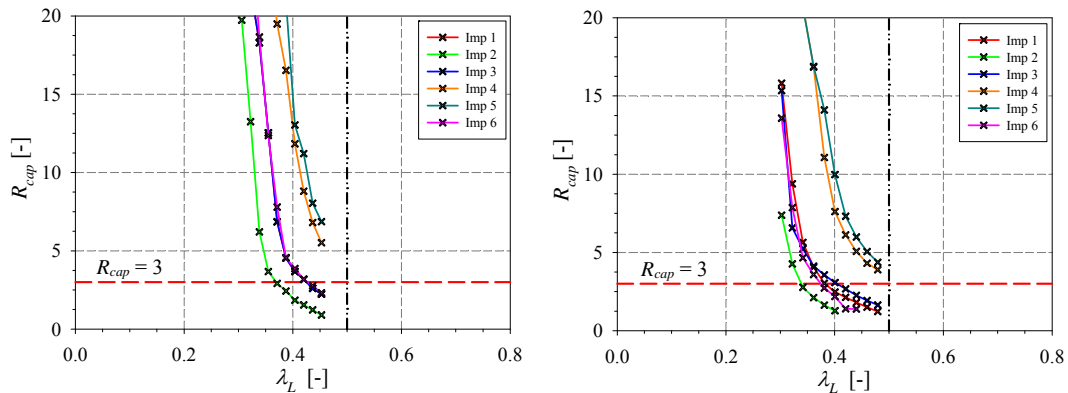
Figure 12: Rotation capacity of hot-rolled hollow sections for different geometrical imperfection patterns – a) Square sections – b) Rectangular sections with $h / b = 2.5$

2.3 Validation against test data

The ability of the developed models to provide reliable reference results was confronted to two experimental series. The 1st test series consisted in some 23 own tests in either simply supported or propped-cantilever configurations, on both hot-finished or cold-formed sections, either

square or rectangular. Typical preliminary measurements such as material response or stub column testing as well as detailed description and analysis of these tests are provided in Saloumi (2017) and shall no longer be detailed here. These data were used to assess the developed shell F.E. models, and the numerical models were shown to quite satisfactorily reproduce the experimental behaviour, in terms of initial stiffness, peak loads, rotational capacity and failure modes. Fig. 13a and 13b recall two examples of moment-rotation curves for a rectangular section RHS 220x120x603 in 3-point bending, and for a square SHS 180x8 in 4-point bending, respectively.
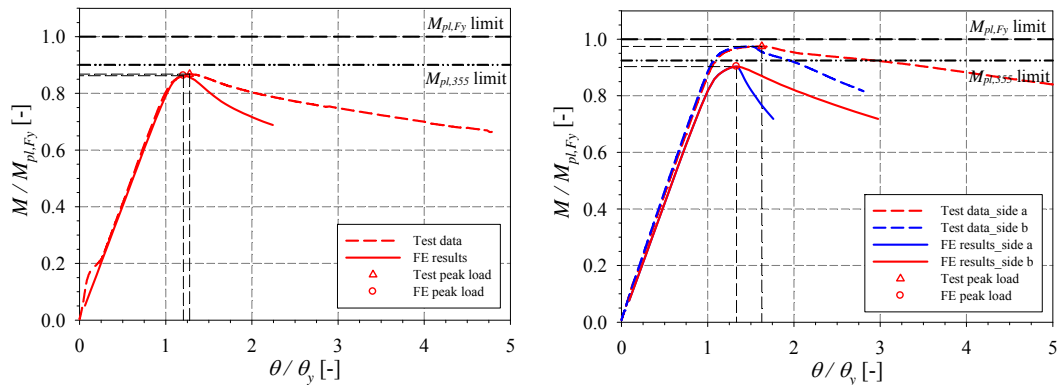

Figure 13: Examples of test vs. F.E. results (Saloumi 2017) – a) Specimen RHS_220×120x6.3_SS_3P – b) Specimen SHS_180x8_SS_4P

As a summary of the test vs. F.E. comparison for this test series, Fig. 14a and14b histograms report on the overall performance of the numerical models vs. test data, in reporting the M_{exp} / M_{FEM} ratio of each test performed. As can be seen, very good agreement is observed, as the predicted failure loads (i) lie in average within 5% of the measured ones, (ii) are generally safe-sided and (iii) never exceed 11%.
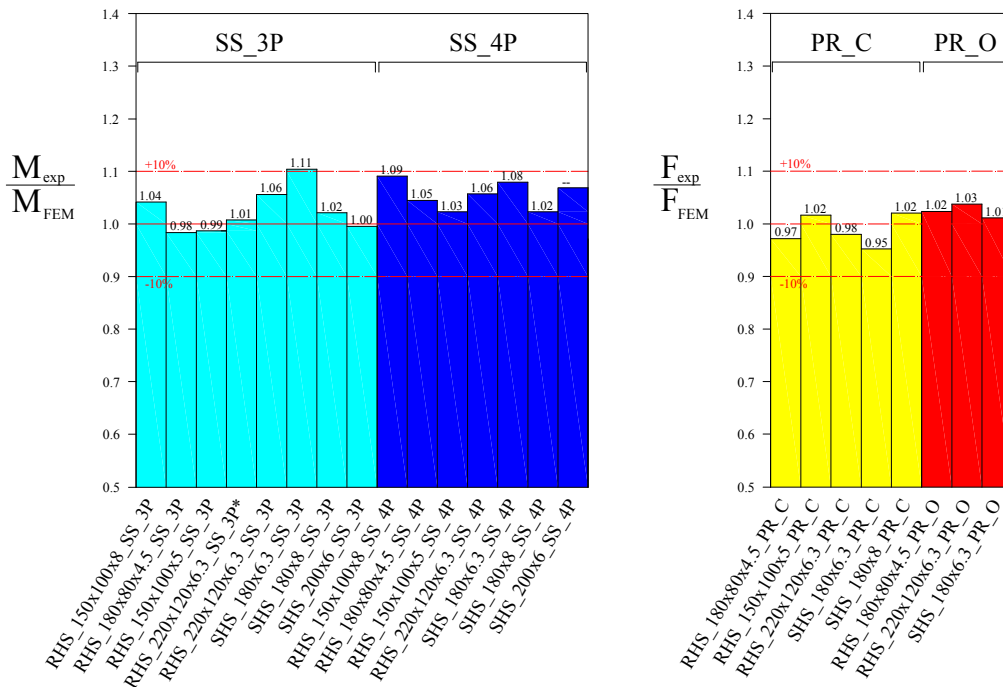

Figure 14: Summary of test vs. F.E. results (Saloumi 2017) – a) Simply-supported configurations – b) Propped-cantilever configurations

In an effort to assess the F.E. models predictions towards additional test data, the results of Wilkinson's experimental series were used as well (Wilkinson 1999). Measured geometric dimensions were implemented, and simple Ramberg-Osgood material law was used for the flat regions of the rectangular hollow sections with material parameter $n = 22$. As Wilkinson reported that the yield stress in flanges was on average 10% higher than that of the webs and 20% higher in the corner regions due to the cold forming process, 1.1 times the measured F_y was considered in the flange regions and a multi-linear law was used for corner regions – the corresponding yield and tensile stresses were equal to 1.2 F_y and 1.2 F_u, respectively. Flexural residual stresses were also implemented and geometrical imperfection pattern Type 1 was introduced in a preliminary-tested sufficiently dense mesh.

Replicating support and loading conditions were achieved through modelling loading plates at loading positions and in the support zones – elastic material behaviour was considered for these plates. Loading was applied at the mid-section location and on all nodes of both webs (Fig. 15). As for support conditions, pinned conditions were attributed to end supports using kinematic linear constraints.
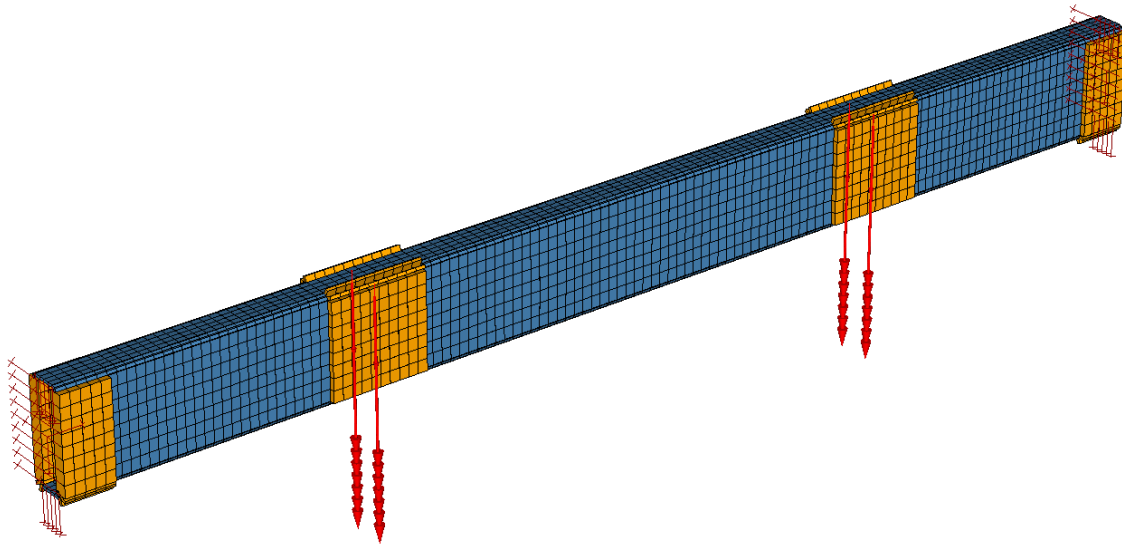

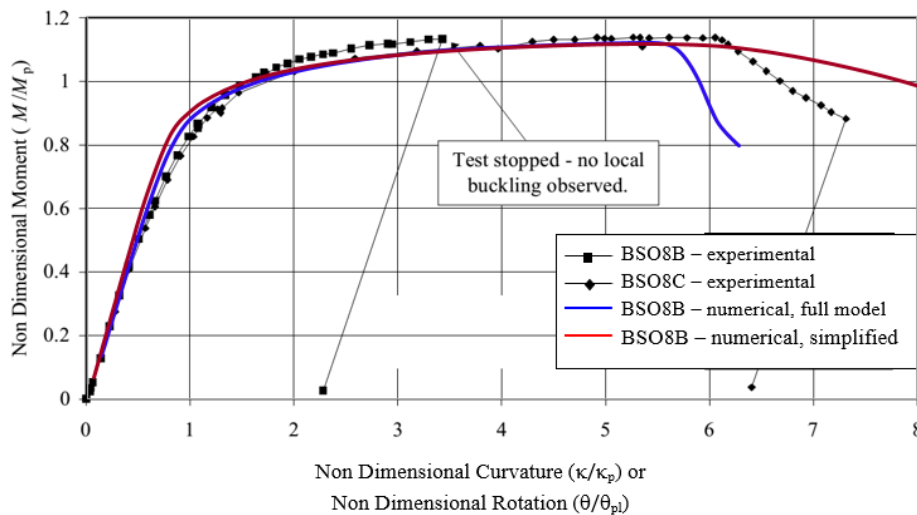Figure 15: Numerical model of Wilkinson 4-pt bending test through "parallel plates" (1999)

Figure 16: Examples of test vs. F.E. results for specimen BS08B

11

Besides, Wilkinson's data have been also used to assess a simplified numerical model. This model consisted in a short beam of length equal to the three times the average of the clear width of both webs and flanges, where loading was introduced through equal bending moments applied at both ends (Fig. 7b), so as to get a constant bending moment distribution. Intention was to validate situations of constant bending moment loading without resorting to the modelling of full 4-pt bending arrangements.

Fig. 16 proposes an example of experimental-numerical comparison results, where both the full model – Fig. 15 – or a simplified one are considered. As can be observed, both numerical curves nicely match the experimental one in the elastic range as well as along the plastic response and for peak loads. In this case, experimental R_{cap} values presented 6% deviation values from both numerical values, an upper one for the simplified model and an under-prediction for the full model.

Fig. 17 finally summarizes the results of the comparison between Wilkinson's 32 experimental and numerical sources – the results of "full" models are reported here. The numerical models are seen to provide fully satisfactory results, with an average deviation of 3% and very few differences exceeding 10%. Accordingly, the numerical models are again shown to possess the ability to provide accurate and reliable results and they shall further be considered as a consistent source of reference results.
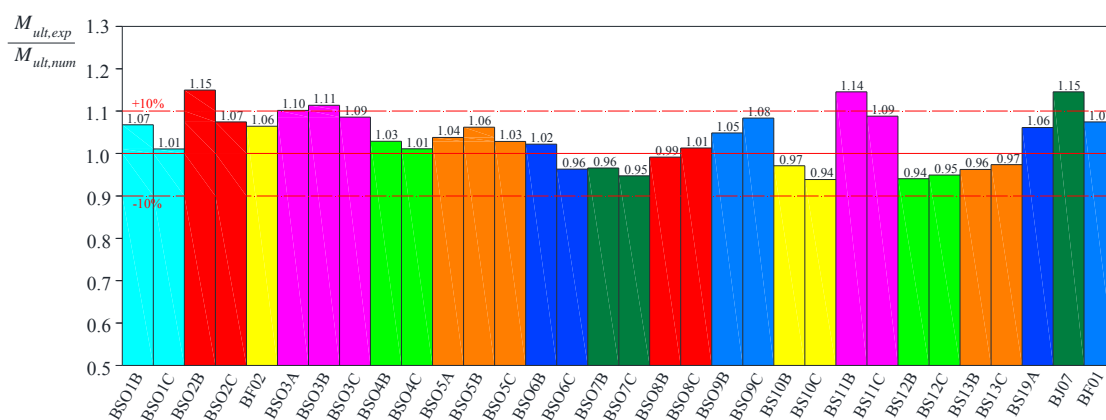

Figure 17: Summary of test vs. F.E. results – Wilkinson's experimental data (1999, 32 tests)

3 Numerical parametric studies – Assessment of λ_L-based criterion

3.1 Parametric studies

The validated F.E. models have been used extensively in numerical parametric studies so as to characterize the dependency of the rotational capacity to various parameters. In this respect, the following variable characteristics were considered in the numerical investigations:

- Material: 3 steel grades were accounted for – S235, S355 and S460 –, simulating the characteristics of hot-finished (Fig. 5) or cold-formed tubes (Figs. 6a and 6b). Depending on the steel grade and on the manufacturing process, differences in plastic plateau length and adequate strain limits were considered;
- Load cases consisted in:
  - Constant bending moment situations (i.e. no moment gradient and no shear action), for which a preliminary length influence study was performed to assess the most suitable length to give the models in order to record little influence of the edge conditions while providing accurate results. Accordingly, beam lengths

of 3 times the averages of the webs and flanges clear widths were assumed here, and use of the simplified model was preferred for saving computation time;

- o 3-point bending arrangements, where the influence of shear and moment gradient could be accounted for. Lengths of 10, 15 and 20 times the height of the cross-section were included in the study, so as to test the influence of moment gradient – use of "full" models was made;

- Section shapes and dimensions were selected to be of class 1 (plastic) or class 2 (compact), according to Eurocode 3 (2005). Many different sections were considered:
  - o Geometries from the European database satisfying the condition $\lambda_p < 0.6$ were first selected;
  - o Invented sections were then generated, on the basis of an $h = 200$ mm section for which h / b ratios were set equal to 1, 1.5, 2, and 2.5, i.e. sections ranged from square to narrow rectangular sections. For each h / b value, b / t quotients ranging from 10 to 20 with a step of 1 and from 20 to 34 with a step of 2 were considered.

Residual stresses – as detailed in § 2.1 – as well as local geometrical imperfection pattern #1 were included in the models; no global geometrical imperfection was accounted for. In total, several hundreds of non-linear F.E. calculations were performed, the results of which are analysed and detailed in the following paragraphs.

3.2 Influence of aspect ratio h / b

As a first parameter suspected to be of influence on the rotational capacity, the height-to-width ratio h / b was investigated – the latter was indeed shown important in the resistance response of both H.S.S. sections (Nseir 2015) and members (Hayeck 2016). Figs. 18a and 18b provide examples of the obtained results, for both hot-finished and cold-formed sections in S235 steel under constant bending moment. Results are plotted in R_{cap} vs. λ_L axes, and $R_{cap} = 3$ horizontal lines are reported to serve as a convenient reference. It shall also be mentioned here that $R_{cap} > 20$ results are not displayed because they could be shown to involve strains higher than 15% at failure, which does not comply with Eurocode 3's material requirements.
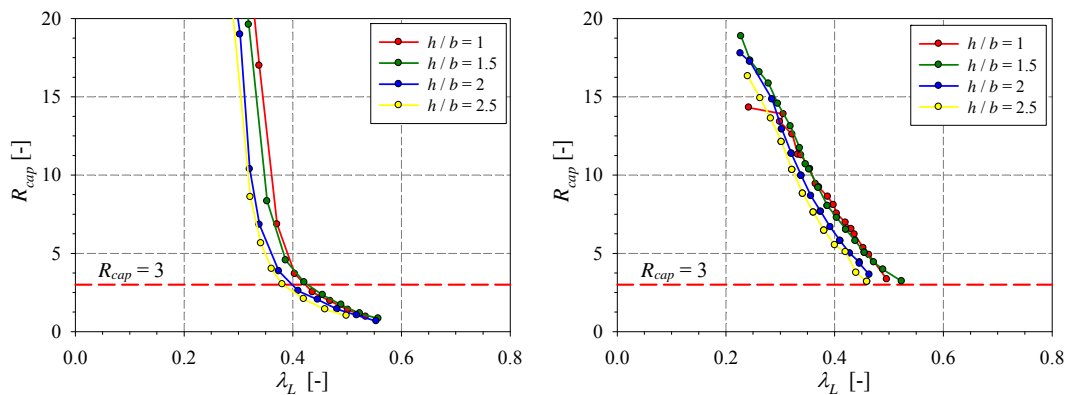

Figure 18: Effect of h / b aspect ratio on R_{cap} (S235, constant bending moment) – a) Hot-finished sections – b) Cold-formed sections

As can be seen, for both hot and cold manufacturing processes, sections possess higher rotation capacities when their shape is closer to square sections. Relative little variations in R_{cap} are however reported, and, given the sensitivity of R_{cap} to many other parameters, including some impossible to master (e.g. geometrical imperfections, see § 2.2), it is suggested that $R_{cap} = f^o(\lambda_L, \ldots)$ sought expressions shall be made free of any h / b coefficient.

3.3 Influence of loading – Moment gradient

Fig. 20 compares the flexural behaviour of beams under constant bending moment and in 3-point bending configurations. As the figure shows, the constant moment cases systematically provide larger rotational capacities than the point load cases, for a given slenderness λ_L. This was expected since a moment gradient triggers a more confined region of maximum moment, so that the still elastic adjacent segments provide a certain level of restraint. Accordingly, yielding and local buckling of the yielded fibres that have lost stiffness cannot spread freely along the beam length, contrary to constant moment cases where local buckling may develop with no such restrictions. For this reason, lower rotation capacities (i.e. less ductile behaviour) shall be reached for 3-point bending arrangements; similar observations and conclusions have been drawn by Lay (1965), Lay et al. (1967), Wang et al. (2016) or Kuhlmann (1989).
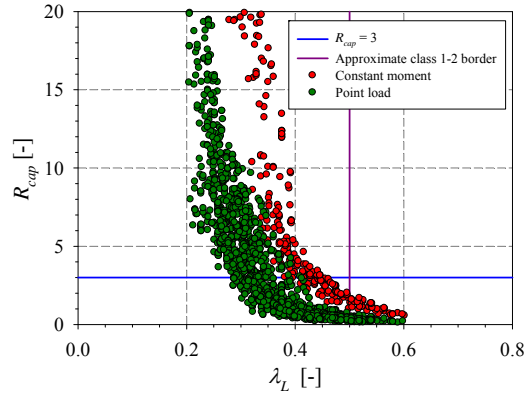

Figure 20: Rotation capacities for beams under: a) Constant moment – b) 3-point bending (hot-finished sections)

Of interest is also the correlation between the rotational capacity reference limit $R_{cap} = 3$ and the slenderness-based limit $\lambda_L = 0.5$ (Eurocode 3, 1989) that is assumed to – approximately – separate class 1 sections (plastic analysis allowed) from class 2 sections (plastic analysis *not* allowed). Sections characterised by both $R_{cap} \geq 3$ and $\lambda_L \leq 0.5$ (data points in the upper left quadrant) are de facto allowing plastic analysis; similarly, sections of the bottom right quadrant ($R_{cap} \leq 3$ and $\lambda_L \geq 0.5$) are judged not to possess the sufficient ductility to allow for plastic redistribution.

More "problematic" are the many data points of the bottom left quadrant: such cases do not possess a rotational capacity above the $R_{cap} = 3$ threshold but satisfy the other $\lambda_L < 0.5$ criterion: a first contradiction is here evidenced, and the two possibilities for allowing plastic analysis are seen not equivalent, especially for point load cases – the $R_{cap} = 3$ criterion is seen more conservative. A suitable alternative criterion should therefore not only account for the effect of moment gradient but also provide adequate solutions for these situations.

3.4 Influence of L / h ratio

For 3-point bending cases, provided the beam member is long enough (this was always the case in the present study), the influence of shear on the formation of plastic mechanisms is known of little influence – particularly in the case of H.S.S. sections characterized by two webs and a uniform thickness for all constituent plates. Varying the length-to-height ratio L / h however influences the moment gradient, so that elastic restraints from zones adjacent to the plastic hinge under consideration may affect the rotational capacity.

Fig. 21 again plots $R_{cap} = f°(\lambda_L)$ results, sorted by length-to-height ratios. It shows that higher rotation capacities are reached for smaller L / h ratios, owing to higher moment gradient that

enable a greater participation of strain hardening, so that sections may sustain their plastic capacity along larger rotations.
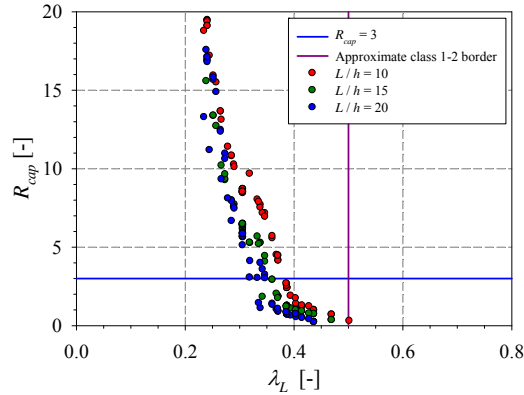

Figure 21: Rotation capacity as influenced by L/h ratio for square, hot-finished sections in 3-point bending (S235)

Also, it is well-known that buckled regions – at mid-span for 3-point configurations – are of nearly constant length but shall be associated to relatively smaller yielded areas thanks to the moment gradient and the restraints from elastic adjacent segments. Therefore, specimens with a steep moment buckle at later stages and provide a greater amount of deformation capacity, which is precisely what the numerical results show. This observation was also evidenced bot experimentally and theoretically by Ricles et al. (1998), Lay et al. (1967), Kuhlmann (1989) or Wang et al. (2016). Since both influences shall be involved in the definition of R_{cap}, dependency of the rotational capacity on length is obvious, and deformations caused by local buckling shall have more importance for short span beams.

3.5 Effect of yield stress and material strain hardening

Fig. 22a reports on the results obtained for hot-finished tubes under constant bending moment, sorted by steel grade. As can be observed, differences remain negligible, and the influence of F_y as included in the calculation of λ_L is seen sufficient.
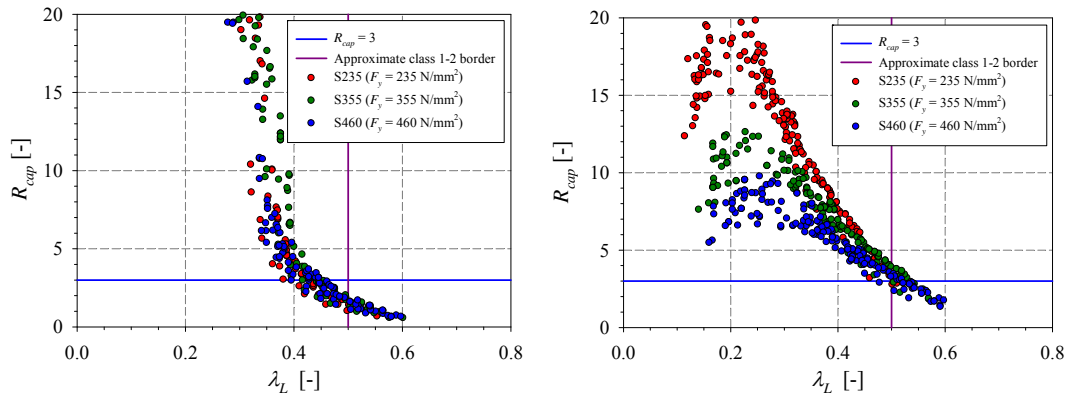

Figure 22: Influence of steel grade on R_{cap} (constant moment) – a) Hot-finished sections – Cold-formed sections

Detailed analysis of these results showed that sections for which $0.35 \leq \lambda_L \leq 0.6$ did not reach significant levels of strain hardening, and failed slightly before reaching their plastic capacity M_{pl}. This explains the very steep increase of R_{cap} noted for $\lambda_L < 0.4$ sections: for the latter, as λ_L decreases, an increasing quantity of fibres gets concerned with yielding, and, given the plastic plateau characteristics, rather suddenly reaches high strains, i.e. the amount of ductility

rises abruptly, and so does R_{cap}. It may be mentioned here that R_{cap} values as high as 50 were recorded but are purposely not displayed, for reasons detailed previously. Finally, one may notice the higher R_{cap} values for S355 steel, which are explained by a relative smaller plastic plateau length (see Fig. 5) leading "faster" to higher strains.

Cold-formed tubes exhibited lower levels of rotational capacity since such sections reach lower strain levels, owing to the rounded material response. Distinct trends can be observed for the various grades, in large extents due to different ultimate-to-yield stress ratio (tangent modulus in strain hardening regime). Scattering in the results at low slenderness for a given steel grade arises from different post-buckling responses. When λ_L gets higher, local buckling becomes prominent and nearly no differences between steel grades are visible, as all materials share the same Young's modulus values. Lower R_{cap} values observed for higher steel grades and very stocky sections ($\lambda_L < 0.25$) shall be associated to the corners possessing relative lower ultimate strains when the yield stress increases, as a result of limiting strains to 2.5% in the corners whatever the steel grade (Fig. 6a): $\varepsilon_{u,corner} = 22.3\ \varepsilon_y$ for S235, $\varepsilon_{u,corner} = 14.8\ \varepsilon_y$ for S355 and $\varepsilon_{u,corner} = 11.4\ \varepsilon_y$ for S235. Consequently, flat faces of S460 grade shall compensate the corners' lack in carrying strains "faster" than for S235 steel in yielding comparatively more, resulting in lower rotational capacities.

Also, a very different response is evidenced for hot-finished sections compared to cold-formed ones, and this is detailed further in the next paragraph.

3.6 Hot-rolled vs. cold-formed H.S.S. response

As already shown, cold-formed sections generally reach lower values of R_{cap} than their hot-finished counterparts at low slenderness. As a result of different manufacturing processes, the material constitutive laws are quite different, namely in terms of (i) strain hardening reserves and (ii) the presence of a plastic plateau for hot-rolled sections.
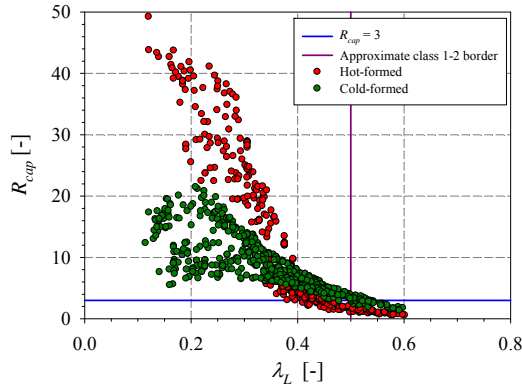

Figure 23: Hot-rolled vs. cold-formed rotation capacity (constant moment)

Fig. 23 indeed shows that for $\lambda_L > 0.4$, preponderant strain hardening reserves in cold-formed sections allow for higher rotational capacities, while the plastic plateau underpins the very high R_{cap} values for $\lambda_L > 0.4$ – Note in particular the amount of high R_{cap} values ($R_{cap} > 20$) for hot-formed sections. Consequently, a proposal for an alternative, slenderness-based criterion to allow for plastic analysis shall make a difference between hot-finished and cold-formed H.S.S.

3.7 Assessment of λ_L-based criterion

Several key parameters with respect to the $R_{cap} = f°(\lambda_L)$ relationship being identified, the present paragraph presents a series of such design equations, for various configurations and cases. Figs. 24a and 24b first show examples on how such design equations have been derived in the

case of hot-finished tubes. As a result of the high slopes observed, a log scale was found more adequate, see Fig. 24a. Then, linear regression analysis allowed to capture the average slope of the results, and adequate shifting permitted the proposal of a lower bound, safe-sided expression. Fig. 24b plots the comparison of the obtained equation with the F.E. results in usual R_{cap}-λ_L axes. For sake of conciseness, all design equations developed are summarised in adequate tables in Section 4 – Table 1 for hot-finished H.S.S.
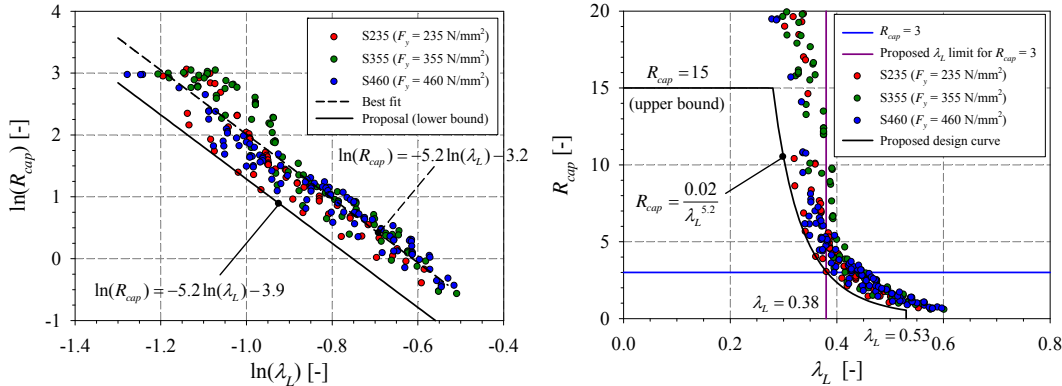

Figure 24: Design equations for hot-finished H.S.S. under constant moment

Two limits have usually been associated to these equations: in the present case, an $R_{cap} = 15$ upper bound limit was fixed so as to restrain the allowable strains and fulfil Eurocode 3 material specifications (2005). Also, a $\lambda_L = 0.53$ limit was established under the assumption that sections potentially considered in a plastic analysis shall show capable of reaching at least 95% of their plastic capacity, otherwise plastic redistributions are deemed impossible. Besides, in the particular example of Fig. 24b, a relative slenderness $\lambda_L \leq 0.38$ is seen to be necessary to fulfil an $R_{dem} \geq 3$ requirement.

A similar approach was followed for deriving design expressions for cold-formed sections. However, due account for (i) lower rotational capacities and (ii) different trends (and slopes) was taken, and two design sets were proposed.

Figure 25: Design equations for cold-formed sections under constant moment – a) Fully detailed method – b) Semi-detailed method (single curve)

A refined, accurate and realistic set of design equations was first proposed, and is summarized as "Method 3: fully detailed method" in Table 2. It accounts for both the ascending then descending trends observed (Saloumi 2016), and remains lower-bounded. Fig. 25a confronts the proposed equations to the numerical results and shows a general safe, good agreement. In

17

the particular case of cold-formed hollow sections, a less restrictive $\lambda_L \leq 0.46$ is shown to be required for satisfying an $R_{dem} \geq 3$ condition.

Alternatively, a more simplified approach consisting in a single equation complemented by adequate upper bounds was derived – see Fig. 25b and Table 2. The latter is comparable to the hot-finished H.S.S. case but is upper bounded by R_{cap} values that depend on the steel grade – Note that less data points were considered for calibrating the design curve, see Fig. 25b.

As detailed in § 3.3, different expressions ought to be considered for beams under 3-point bending load cases, and lower $R_{cap} = f°(\lambda_L)$ relationships have been derived accordingly. Fig. 26 shows an example for these situations, where different upper bound limits have been proposed depending on the steel grade, and a $\lambda_L = 0.53$ limit is however maintained.

Figure 26: Design equations for hot-finished H.S.S. under 3-point bending

Eventually, Figs. 27a and 27b plot the proposed equations for cold-formed sections in 3-point bending. Likewise, two different approaches have been proposed, and are summarized in Table 2. Again, a limit $\lambda_L = 0.53$ was shown adequate and kept for full consistency within the various design equations recommended. As for the semi-detailed approach with a single curve, only sections characterised by $\lambda_L > 0.4$ values have been accounted for in the derivation of the design equation. Again, individual upper bounds R_{cap} limits have been fixed as a function of the steel grade, albeit at lower values than for the case of constant bending moment.
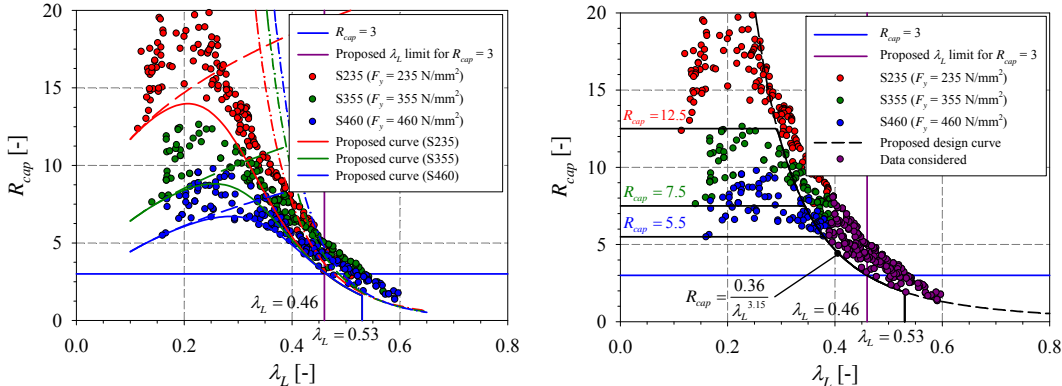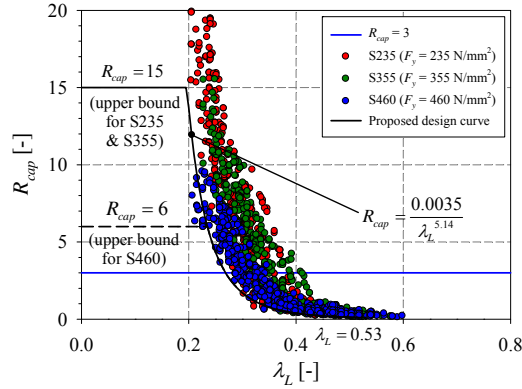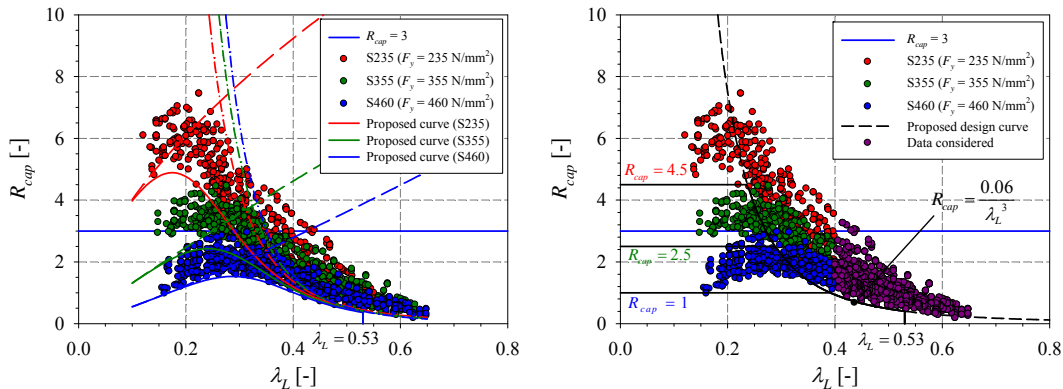

Figure 27: Design equations for cold-formed sections under 3-point bending – a) Fully detailed method – b) Semi-detailed method (single curve)

4 Summary of recommendations

4.1 Hot-finished sections

Table 1 gathers the various design equations developed for hot-finished H.S.S. So-called "Method 1" refers to the simplest λ_L-based criterion ensuring that the section possesses a minimum $R_{cap} = 3$ reserve, capable of satisfying Eurocode 3's underlying $R_{dem} \geq 3$ requirement (1989). The – recommended – Method 2 provides more accurate and specific R_{cap} expressions, for different yield stresses and different load cases; upper bounds as well as "guaranteed" minimum R_{cap} values for sections possessing a local slenderness such that $\lambda_L \leq 0.53$ are also indicated.

Table 1: Design recommendations for hot-finished sections

Method 1 (simplest)				
Sections satisfying $\lambda_L < 0.38$ allow for plastic analysis (ensures $R_{cap} \geq 3$, regardless of R_{dem})				
Method 2: detailed method (R_{dem} is known)				
Load case	Yield stress	Proposed equation	Upper bound	Min. R_{cap} if $\lambda_L \leq 0.53$
Constant moment	$F_y \leq 460$	$R_{cap} = \dfrac{0.02}{\lambda_L^{5.2}}$	$R_{cap\ max.} = 15$	$R_{cap\ min.} = 0.5$
Moment gradient	$F_y \leq 355$	$R_{cap} = \dfrac{0.0035}{\lambda_L^{5.14}}$	$R_{cap\ max.} = 15$	$R_{cap\ min.} = 0.09$
	$355 < F_y \leq 460$		$R_{cap\ max.} = 6$	

4.2 Cold-formed sections

In the same way, design proposals for cold-formed tubes are summarized in Table 2, which refers to the following distinct methods:

- A basic, simple, λ_L-based Method 1 criterion;
- A semi-detailed Method 2 relying on a unique design equation coupled with suitable upper bounds (see § 3.7);
- A more refined and detailed Method 3 that better accounts for the particular shapes of the $R_{cap} = f°(\lambda_L)$ relationships reported for cold-formed sections through specific R_{cap} expressions.

5 Conclusions

This paper focused on proposing alternative criteria to allow for plastic analysis in the particular case of steel H.S.S. profiles. These criteria consist in providing relationships between the section's rotational capacity R_{cap} and its local relative slenderness λ_L that include the influence of key parameters such as the steel grade, load distribution and fabrication process. They have been derived from hundreds of numerical results, based on non-linear shell F.E. models carefully validated against more than 50 bending tests. It was shown that several other parameters such as the height-to-width h/b aspect ratio or the steel grade were not of significant influence and could be avoided in the proposed design expressions. Hot-finished sections were shown to exhibit deeply increasing R_{cap} values when λ_L decreases, as a result of the plastic plateau in the material law, whatever the steel grade. In contrast, cold-formed tubes displayed quite more limited rotational capacities at low slenderness that depend on the material grade, but higher ones for $0.4 \leq \lambda_L \leq 0.6$ which corresponds to the compact sections range, owing to strain hardening effects. Eventually, the proposed design equations are summarized in code-ready tables that suitably complement the recently-developed O.I.C. design approach.

Table 2: Design recommendations for cold-formed sections

Method 1 (simplest)				
Sections satisfying $\lambda_L < 0.46$ allow for plastic analysis (ensures $R_{cap} \geq 3$, regardless of R_{dem})				
Method 2: semi-detailed method (R_{dem} is known)				
Load case	Steel grade	Proposed equation	Upper bound	Min. R_{cap} if $\lambda_L \leq 0.53$
Constant moment	S235	$R_{cap} = \dfrac{0.26}{\lambda_L^{3.15}}$	$R_{cap\,max.} = 12.5$	$R_{cap\,min.} = 1.9$
	S355		$R_{cap\,max.} = 7.5$	
	S460		$R_{cap\,max.} = 5.5$	
Moment gradient	S235	$R_{cap} = \dfrac{0.06}{\lambda_L^{3}}$	$R_{cap\,max.} = 4.5$	$R_{cap\,min.} = 0.4$
	S355		$R_{cap\,max.} = 2.5$	
	S460		$R_{cap\,max.} = 1$	
Method 3: fully detailed method (R_{dem} is known)				
Load case	Steel grade	Proposed equation	Upper bound: $\lambda_L \leq 0.1$	Min. R_{cap} if $\lambda_L \leq 0.53$
Constant moment	S235	$R_{cap} = \dfrac{1}{\dfrac{1}{25\lambda_L^{0.33}} + \dfrac{\lambda_L^{5.2}}{0.065}}$	$R_{cap\,max.} = 11.7$	$R_{cap\,min.} = 1.6$
	S355	$R_{cap} = \dfrac{1}{\dfrac{1}{16.5\lambda_L^{0.41}} + \dfrac{\lambda_L^{5.9}}{0.043}}$	$R_{cap\,max.} = 6.4$	$R_{cap\,min.} = 1.6$
	S460	$R_{cap} = \dfrac{1}{\dfrac{1}{12.8\lambda_L^{0.46}} + \dfrac{\lambda_L^{6.4}}{0.033}}$	$R_{cap\,max.} = 4.4$	$R_{cap\,min.} = 1.6$
Moment gradient	S235	$R_{cap} = \dfrac{1}{\dfrac{1}{16\lambda_L^{0.6}} + \dfrac{\lambda_L^{4}}{0.035}}$	$R_{cap\,max.} = 4.0$	$R_{cap\,min.} = 0.4$
	S355	$R_{cap} = \dfrac{1}{\dfrac{1}{10.6\lambda_L^{0.9}} + \dfrac{\lambda_L^{4.5}}{0.023}}$	$R_{cap\,max.} = 1.3$	$R_{cap\,min.} = 0.4$
	S460	$R_{cap} = \dfrac{1}{\dfrac{1}{8.2\lambda_L^{1.2}} + \dfrac{\lambda_L^{4.9}}{0.018}}$	$R_{cap\,max.} = 0.6$	$R_{cap\,min.} = 0.4$

6 References

AISC (2010). "Specification for structural steel buildings", American Institute of Steel Construction, Chicago, IL. ANSI/ASIC 360-10 & AISC Design Guide 27 (2013), "Structural Stainless Steel".

AS 4100 (1998). "Australian Standard AS 4100 Steel Structures".

Boissonnade, N., Nseir, J., Hayeck, M., Saloumi, E. (2014). "Predicting steel member carrying capacity by means of the Overall Interaction Concept", Proceedings of the 7th European Conference on Steel Structures, Eurosteel 2014, Naples, Italy.

Boissonnade, N., Hayeck, M., Saloumi, E., Nseir, J. (2017). "An Overall Interaction Concept for an alternative approach to steel member design", Journal of Constructional Steel Research, vol. 135, pp. 199-212.

Chen, Y., Cheng, X., Nethercot, D. (2013). "An overview study on cross-section classification of steel H-sections", Journal of Constructional Steel Research, Vol. 80, pp. 386-393.

Dawson, R. G., Walker, A. C. (1972). "Post-buckling of geometrically imperfect plates", Journal of the Structural Division, ASCE, vol. 98, No. 1, pp. 75–94.

Eurocode 3 Editorial Group (1989). "The b / t Ratios Controlling the Applicability of Analysis Models in Eurocode 3", Document 5.02, Background Documentation to Chapter 5 of Eurocode 3, Aachen University, Germany.

European Committee for Standardisation (2005). EN 1993-1-1: Eurocode 3 – Design of steel structures. Part 1.1: General rules for buildings. CEN Brussels.

Galambos, T. V. (1968). "Deformation and energy absorption capacity of steel structures in the inelastic range", Journal of Constructional Steel Research.

Gardner, L., Saari, N., Wang, F. (2010). "Comparative experimental study of hot-rolled and cold-formed rectangular hollow sections", Thin-Walled Structures, vol. 48, No. 7, pp. 495–507.

Greisch Design Office, University of Liège. (1999). "FINELg, Non Linear Finite Element Analysis Software".

Hasan, S. W., Hancock, G. J. (1989). "Plastic Bending Tests of Cold-Formed Rectangular Hollow Sections".

Hayeck, M., Nseir, J., Saloumi, E., Boissonnade, N. (2015). "Use of Ramberg-Osgood material laws in the finite element modeling of cold-formed tubes", Proceedings of the 15th International Symposium on Tubular Structures ISTS15, Rio de Janeiro, Brasil.

Hayeck, M. (2016). "Development of a New Design Method for Steel Hollow Section Members Resistance", PhD thesis, University of Liège, Belgium.

Hayeck, M., Nseir, J., Saloumi, E., Boissonnade, N. (2018). "Experimental characterization of steel tubular beam-columns resistance by means of the Overall Interaction Concept", Thin-walled Structures, Vol. 128, pp. 92-107.

Kato, B. (1989). "Rotation capacity of H-section members as determined by local buckling", Journal of Constructional Steel Research, Vol. 13, pp. 95-109.

Kemp, A. R. (1984). "Slenderness limits normal to the plane of bending for beam-columns in plastic", Journal of Constructional Steel Research, Vol. 4, pp. 135-150.

Korol, R. M., Hudoba, J. (1972). "Plastic Behavior of Hollow structural sections", Journal of the Structural Division, American Society of Civil Engineers, Vol. 98, No 5, pp 1007-1023.

Kuhlmann, U. (1989). "Definition of flange slenderness limits on the basis of rotation capacity values", Journal of Constructional Steel Research, Vol. 14, No. 1, pp. 21–40.

Lay, M. G. (1965). "Some studies of flange local buckling in wide-flange shapes", Proceedings ASCE, Vol. 91, ST6, Publication No. 288.

Lay, M. G., Galambos, T. V. (1967). "Inelastic beams under moment gradient", Journal of the Structural Division, ASCE.

Merchant, W. (1954). "The failure load or rigidly jointed frame works as influenced by stability", The Structural Engineer, Vol. 32.

Neal, B. G. (1977). "The plastic methods of structural analysis", London; New York: Chapman and Hall ; Wiley.

Nseir, J. (2015). "Development of a New Design Method for the Cross-section Capacity of Steel Hollow Sections", PhD thesis, University of Liège, Belgium.

Ricles, J. M., Sause, S., Green, P. S. (1998). "High-strength steel: implications of material and geometric characteristics on inelastic flexural behavior", Engineering Structures, Vol. 20, pp. 323–335.

Saloumi, E. (2016). "Development of a new design method to define the rotation capacity of steel hollow sections", Ph.D. thesis, University of Liège, Belgium.

Saloumi, E., Hayeck, M., Nseir, J., Boissonnade, N. (2017). "Experimental and numerical characterization of HSS rotational capacity", Proceedings of the SSRC Annual Stability Conference, San Antonio, U.S.A.

Stranghoner, N., Sedlacek, G., Boeraeve, P. (1994). "Rotation requirement and rotation capacity of rectangular, square and circular hollow section beams", Tubular structures VI, Grundy, Holgate & Wong (eds).

Wang, J., Afshan, S., Gkantou, M., Theofanous, M., Baniotopoulos, C., Gardner, L. (2016). "Flexural behaviour of hot-finished high strength steel square and rectangular hollow sections", Journal of Constructional Steel Research, Vol. 121, pp. 97-109.

Wilkinson, T. (1999). "The Plastic Behaviour of Cold-Formed Rectangular Hollow Sections", PhD thesis, the university of Sydney.

Yun, X., Gardner, L. (2017). "Stress-strain curves for hot-rolled steels", Journal of Constructional Steel Research, Vol. 133, pp 36-46.

Yura, J., Galambos, T. V., Ravindra, M. (1978). "The bending resistance of steel beams", Journal of the Structural Division.

Zhao, X. L., Hancock, G. J. (1991). "Tests to determine plate slenderness limits for cold-formed rectangular hollow sections of grade C450", Journal of the Australian Steel Institute, Vol. 25, No 4, pp. 2-16.

Ziemian, R. D., McGuire, W., Deierlein, G. G. (1992). "Inelastic limit states design, Part I: Planar frame studies", Journal of Structural Engineering, ASCE, Vol. 118, No 9, pp. 2532–2549.